Attitude Determination of a Spin-Stabilized Lunar Satellite

WILLIAM O. COVINGTON JR.*
Bellcomm Inc., Washington, D. C.

A KALMAN filter can be used to estimate the attitude of a spin-stabilized lunar satellite, based on sun aspect angle measurements made periodically by a single sun sensor on the satellite and telemetered to the ground for processing. Spin axis attitude information is required to an accuracy of about 1% on certain scientific satellites for the proper interpretation of magnetometer data. The sun sensor used in this analysis measures the angle between the satellite axis of symmetry and a line of sight to the sun. The measured quantity is a planar angle, and the filter is used to generate a two-dimensional estimate of the spin axis orientation.

The system dynamics, consisting of the precession of the satellite angular momentum vector in response to the lunar gravity gradient torque, is influenced indirectly by the anomalies in the lunar gravity field. The oblateness and higher order terms cause changes in the satellite orbital elements which in turn influence the gravity gradient torque. If the lunar gravity field were spherical and the Earth and sun were not present, the orbit plane would remain fixed in space, and the satellite angular momentum vector would precess about a normal to the orbit plane in a manner similar to the precession of the equinoxes of the earth. However, the nonspherical lunar gravity field and the gravity field of the Earth cause changes in the elements of the orbit, which affects the satellite attitude relative to the lunar gravity field. This effect influences substantially the gravity gradient torque acting on the satellite.

The analysis presented here uses a computer statistical simulation of a Kalman filter attitude estimator. A characteristic of the Kalman filter is that the estimated state error covariance matrix depends upon the initial value of this matrix, the estimated measurement error covariance matrix and the measurement schedule, and is independent of the actual measurements. This characteristic can be used to simulate the performance of the filter without actually making measurements. The results indicate the uncertainty in the attitude error, assuming that the initial attitude error covariance matrix and the measurement error estimates used in the simulation correctly represent the corresponding real-world quantities and that the system dynamics model is valid.

Development of Precession Rate Equations

The orientation of the satellite momentum vector is described by the angles θ and ψ in the selenocentric inertial coordinate system shown in Fig. 1. Here the acceleration of the origin can be ignored. Vectors $\mathbf{e}_1$, $\mathbf{e}_2$, $\mathbf{e}_3$ are unit vectors in the selenocentric inertial coordinates. Unit vector $\mathbf{u}_E$ is normal to the ecliptic plane; unit vector $\mathbf{u}_L$ lies along the satellite spin angular momentum vector, $\mathbf{L}$; and unit vector $\mathbf{u}_s$ is directed toward the sun. The gravity gradient torque will be described in terms of the $\mathbf{v}_1, \mathbf{v}_2, \mathbf{v}_3$ right-hand, orthogonal unit vectors where $\mathbf{v}_3$ lies along $\mathbf{u}_L$ and $\mathbf{v}_1$ lies in the xy plane. The satellite is assumed to be a rigid body spinning about its axis of symmetry. The satellite spin rate is assumed constant, so that $\dot{L}_k = 0$ in the rotation dynamics equation, $\mathbf{N} = \dot{\mathbf{L}} = \mathbf{b}_k\dot{L}_k + \mathbf{W} \times \mathbf{L}$, which reduces to $\mathbf{N} = \mathbf{W} \times \mathbf{L}$, where $\mathbf{N}$ = torque vector, $\mathbf{L}$ = angular momentum vector = $\mathbf{v}_3 L$, $\mathbf{b}_i$ = unit base vectors in satellite body axes, $\dot{L}_k$ = components of rate of change of the magnitude of the satellite momentum vector, $\mathbf{W}$ = satellite angular velocity vector = $\mathbf{v}_1\dot{\theta} + \mathbf{v}_2\dot{\psi}\sin\theta + \mathbf{v}_3\dot{\psi}\cos\theta$.

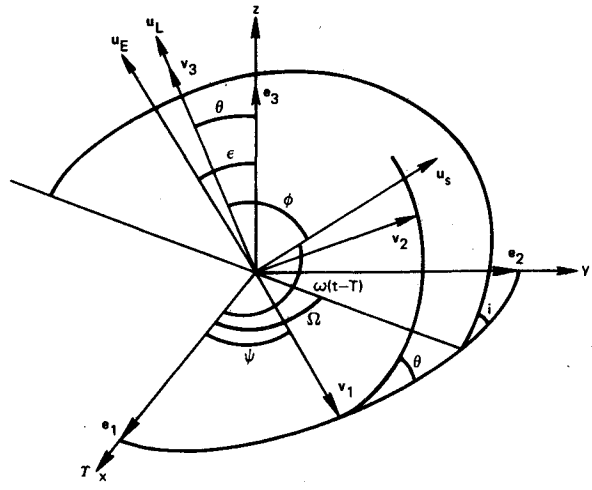

Fig. 1 Geometry of vectors for attitude estimation.

The disturbing torques due to earth-gravity gradient, sun-gravity gradient, magnetic moment, lunar oblateness, and solar radiation pressure were all considered and dropped. The largest of those, the solar radiation torque, which can be a significant fraction of the lunar-gravity gradient torque, can be either modeled in the attitude determination filter or suppressed with special vehicle design.

The gravity gradient torque on the satellite averaged over one period is[1]

$$\mathbf{N} = F\{[\sin i\cos\theta\cos(\Omega - \psi) - \cos i\sin\theta]\mathbf{v}_1 + \sin i\sin(\Omega - \psi)\mathbf{v}_2\} \quad (1)$$

where

$$F = [6\pi^2(I_3 - I)/T_n^2(1 - e^2)^{3/2}][\cos i\cos\theta + \sin i\sin\theta\cos(\Omega - \psi)]$$

and I_3 = moment of inertia of satellite about its spin axis, I = moment of inertia transverse to spin axis, T_n = period of orbit, e = eccentricity, i = inclination of orbit, and Ω = ascending node of orbit. The precession rates are given by

$$\dot{\psi} = (F/L\sin\theta)\,[\sin i\cos\theta\cos(\Omega - \psi) - \cos i\sin\theta] \quad (2)$$

$$\dot{\theta} = -F/L\sin i\sin(\Omega - \psi) \quad (3)$$

These angular rates were numerically integrated in the computer program to produce the satellite spin axis Euler angles. A computer program was used to generate and tabulate the orbital elements as a function of time for the $L-1$ lunar gravity model[2] augmented with the perturbation effect of the Earth's gravity. This element tableau was sampled periodically and interpolated to obtain elements for the gravity gradient torque expression. A computer program was used to integrate numerically the precession rate equations and to

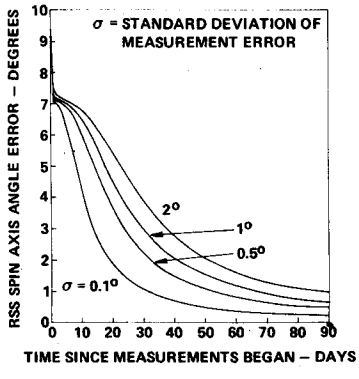

Fig. 2 Estimated spin axis attitude error for 10° initial error.

Received March 9, 1971; revision received June 10, 1971.
Index category: Spacecraft Attitude Dynamics and Control.
* Member Technical Staff, Guidance and Navigation Department. Member AIAA.

produce the orientation of the spin axis as a function of time. One orbital period was used as the integration interval, and the spin axis orientation angles were recorded at one day intervals. The initial elements used in the simulation were Ω = ascending node = $-171.99°$, i = inclination = $146.42°$, a = semimajor axis = 6.066961924×10^6 ft, and e = eccentricity = 0.001, typical of an Apollo spacecraft orbit.

Kalman Filter Attitude Estimator Equations

For the Kalman filter, the system was modeled as a state equation and a measurement relation.

$$\dot{\mathbf{x}} = f(\mathbf{L},\mathbf{N}) \tag{4}$$

$$\phi = \phi(\mathbf{x},\mathbf{u}_s,\nu) \tag{5}$$

where: $\mathbf{x}^T = [\theta,\psi]$ = state vector, ϕ = measured solar aspect angle, $\mathbf{u}_s$ = unit vector directed toward the sun, and ν = Gaussian measurement noise. Equation (4) is given by Eqs. (2) and (3). The measurement relation can be developed from the vectors of Fig. 1. The unit vector along the spin axis of the satellite is given by

$$\mathbf{u}_L = \mathbf{e}_1 \sin\theta \sin\psi - \mathbf{e}_2 \sin\theta \cos\psi + \mathbf{e}_3 \cos\theta \tag{6}$$

The unit vector directed toward the sun is normal to $\mathbf{u}_E$ and is given by

$$\mathbf{u}_s = \mathbf{e}_1 \cos\omega(t - T) + \mathbf{e}_2 \sin\omega(t - T) \cos\epsilon + \mathbf{e}_3 \sin\omega(t - T) \sin\epsilon \tag{7}$$

where ϵ = obliquity of the ecliptic $\approx 23.45°$, ω = mean orbital rate of the Earth about the sun, $t - T$ = time from vernal equinox passage, T = time of vernal equinox passage. In a real-time filter, the sun direction vector would be determined from ephemeris data rather than the mean orbital rate of the Earth. The cosine of the measured sun aspect angle is given by $\cos\phi = \mathbf{u}_L \cdot \mathbf{u}_s$.

The Kalman filter equations have been described in numerous places and are given by Ref. 3

$$\hat{x}_n = \bar{x}_n + K_n(\tilde{\phi}_n - \bar{\phi}_n) \tag{8}$$

$$M_n = \Phi_{n,n-1} P_{n-1} \Phi^T_{n,n-1} \tag{9}$$

$$K_n = P_n H_n{}^T R_n{}^{-1} \tag{10}$$

$$P_n{}^{-1} = M_n{}^{-1} + H_n{}^T R_n{}^{-1} H_n \tag{11}$$

where $\hat{x}_n$ = estimate of the state vector at stage n taking into account the measurements $\tilde{\phi}_n$, $\bar{x}_n$ = estimate of the state vector before measurements are made, $\bar{\phi}_n$ = estimate of the measurements based on state estimate $\bar{x}_n$, $H_n = [\partial\phi/\partial\theta, \partial\phi/\partial\psi]$, P_n = estimated covariance matrix of $\mathbf{x}_n$ after incorporation of measurement data, M_n = estimated error covariance matrix before measurement, R_n = estimated covariance matrix of ϕ_n (simply the estimated variance of ϕ in this case, since ϕ is a scalar), $\Phi_{n,n-1}$ = transition matrix of $\mathbf{x}_n$, K_n = filter weighting matrix which minimizes the trace of P_n. The elements of H are derived from the $\cos\phi = \mathbf{u}_L \cdot \mathbf{u}_s$ relation as

$$\partial\phi/\partial\theta = -(1/\sin\phi)(C_1 \cos\theta \sin\psi - C_2 \cos\theta \cos\psi - C_3 \sin\theta) \tag{12}$$

$$\partial\phi/\partial\psi = -(1/\sin\phi)(C_1 \sin\theta \cos\psi + C_2 \sin\theta \sin\psi) \tag{13}$$

where $C_1 = \cos\omega(t - T)$, $C_2 = \sin\omega(t - T) \cos\epsilon$, $C_3 = \sin\omega(t - T) \sin\epsilon$.

The Kalman filter equations provide the minimum variance optimal estimate which is linear in the errors. The covariance matrix propagation with the transition matrix in Eq. (9) implies a linearization of Eq. (4). The filter weighting matrix, K_n, in Eq. (8) linearly relates the state vector estimate to the deviation between the actual measurements and the estimated measurements. The matrix of partial derivatives, H_n, linearly relates the measurement deviation to the state vector deviation from a reference state.

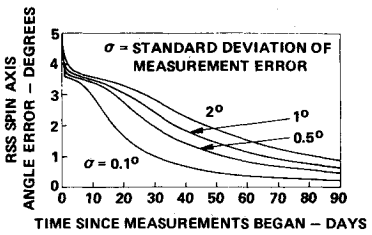

Fig. 3 Spin axis attitude error for 5° initial error.

In the present analysis, Eq. (9) was used to propagate the covariance matrix between measurement points, and Eq. (11) was used to update the covariance matrix at measurement points. The results expressed in terms of orientation angular errors correspond to correctly estimated initial state error and measurement error and to a valid system model.

The spin axis orientation error can be expressed as the root-sum-square of the α and β error components defined as $\alpha \approx \delta\psi \sin\theta$, $\beta \approx \delta\theta$.

$$RSS = (\sigma_\alpha{}^2 + \sigma_\beta{}^2)^{1/2} = (\sigma_\psi{}^2 \sin^2\theta + \sigma_\theta{}^2)^{1/2} \tag{14}$$

Where $\sigma_\alpha{}^2, \sigma_\beta{}^2$ = variances of α, β respectively. These α and β angles are introduced to generate a single-number attitude error estimate for this analysis.

The transition matrix for vector $\mathbf{x}$ must be determined from Eq. (4). This nonlinear equation would yield rather lengthy expressions in linearized form. An alternative is to compute the transition matrix numerically by injecting small variations in the state vector elements, numerically integrating Eq. (4) and differencing the result produced at the later time. This alternative, which was used in this analysis, provided the transition matrix as follows:

$$\Phi_{n,n-1} = \begin{bmatrix} \Phi_{11} & \Phi_{12} \\ \Phi_{21} & \Phi_{22} \end{bmatrix}$$

where

$$\Phi_{11} = [\theta_n(\theta_{n-1} + \Delta\theta, \psi_{n-1}) - \theta_n(\theta_{n-1}, \psi_{n-1})]/\Delta\theta$$

and with corresponding expressions for the other elements. These expressions were used with $\Delta\theta$, $\Delta\psi = \frac{1}{2}°$ in the computer program to generate the transition matrix. The filter simulation was initialized with an estimated state error covariance matrix corresponding to a pointing error apportioned equally in the α and β directions. Initial pointing errors of 5° and 10° were used. Several values of measurement error standard deviation between 0.1° and 2° were used to assess the effect of measurement error on the response time of the filter.

Results

The *RSS* angle estimation error of the spin axis for several values of standard deviation σ of measurement error is shown in Figs. 2 and 3 for initial attitude errors of 10° and 5° respectively, apportioned equally between α and β. The first few measurements reduce the error in the measurement angle plane (plane of ϕ) but have little effect on the error normal to the measurement plane. Consequently, in Fig. 2 the *RSS* error is reduced from its initial 10° value to about 7° and remains there until the spin axis precession and the sunline movement yield a significant component of measurement angle normal to the original angle measurement plane. The curves show that a measurement interval of 30–90 days will be required to reduce an initial 10° attitude uncertainty to a value less than 1°, depending upon the accuracy of the measurements. Comparison of Figs. 2 and 3 shows that the time for the filter to reduce the error to one degree is about the same for both 10° and 5° initial errors, as expected since linear estimation theory is used.

References

[1] Thomas, L. C. and Cappellari, J. O., "Attitude Determination and Prediction of Spin-Stabilized Satellites," *Bell System Technical Journal*, Vol. XLIII, No. 4, July 1964, p. 1680.

[2] Wollenhaupt, W. R., "Apollo Orbit Determination and Navigation," AIAA Paper 70-27, New York, 1970.

[3] Bryson, A. E., Jr. and Ho, Y. C., *Applied Optimal Control*, Blaisdell, 1969, p. 361.

Heat-Transfer Optimization of Convergent Section of a Hypersonic Flow Nozzle

TARIT KUMAR BOSE* AND
T. R. SANKARANARAYANAN†
Indian Institute of Technology, Madras, India

Nomenclature

A = area, m²
a = sonic velocity = $(\gamma RT)^{0.5}$, m/sec
c_p, c_n = isobar and polytropic specific heats, respectively, J/kg-°K
D = diameter, m
g = recovery to stagnation temperature ratio, Eq. (10)
k = coefficient of heat conduction, W/m-°K
L = length of the convergent part of the nozzle, m
M = Mach number
$\dot{m}_0$ = mass flow rate, kg/sec
N = a characteristic number, Eq. (15)
Nu = Nusselt number
Pr = Prandtl number = $\eta c_p/k$
p, p_0 = static and total pressures, respectively, N/m²
Q_m = specific heat load, joule/kg, Eq. (14)
q_m = specific heat addition, joule/kg
q_s = heat flux, W/m²
R = gas constant, joule/kg-°K
Re = Reynolds number = $\rho VD/\eta$
r = recovery factor = $(Pr)^{0.5}$, Eq. (9)
T, T_0 = static and total temperatures, respectively, °K
T_r = recovery temperature, °K
V = gas velocity, m/sec
x = axial length, m
γ = adiabatic exponent
η = dynamic viscosity coefficient, kg/m-sec
λ = Lagrange undetermined multiplier
ρ = density, kg/m³
θ = a dimensionless function, Eq. (15)

Subscripts and superscripts

$( )^*$ = dimensionless quantity
$( )'$ = derivative with respect to axial coordinate
i = nozzle inlet condition
t, w = throat and wall condition, respectively
∞ = freestream condition

Introduction

THE exit Mach number in a coverging-diverging nozzle depends on the square root of ratio of two temperatures—the total temperature at the inlet of the nozzle to the static temperature at the exit. Since the exit static temperature cannot be lowered beyond the saturation temperature of the working gas, an increase in T_{0i}, the total temperature of the working gas at the inlet, is the only way in which the exit Mach number may be increased beyond a certain value. At the nozzle inlet the heating requirement of the gas increases as $P_{0i}A_t(T_{0i})^{0.5}$, whereas the heat flux at the throat region increases as $p_{0i}{}^{0.8}T_{0i}{}^{0.6}A_t{}^{-0.1}$. Thus for a given p_{0i} and A_t, an increase in the exit Mach number results in a proportionate increase in the heating requirement of the gas at the nozzle inlet, whereas the heat flux increases slightly more. Hypersonic nozzles in steady-state operation in general are subjected to very intense heat flux levels, and consequently very high energy losses. The performance of a hypersonic nozzle is dependent strongly on the shape of the convergent part of the nozzle. The design of the divergent part of the nozzle is dependent on some other considerations and has been examined by many authors[1] and is not a part of the present investigation.

Received March 15, 1971; revision received June 2, 1971.
Index category: Nozzle and Channel Flow.

* Associate Professor. Member AIAA.

† Undergraduate Student.

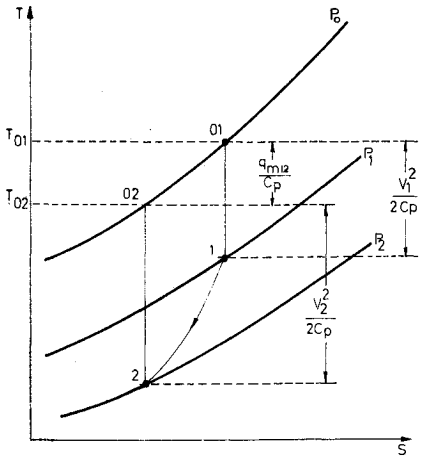

Fig. 1 Effect of heat transfer in an expanding flow on change of state between two points.

The method of the present investigation assumes the nozzle flow to consist of a series of fully developed turbulent pipe flows. Thus each point in the nozzle is assumed to have been preceded by a very long pipe of the local diameter of interest. The method seems to work for nozzles of moderate converging and diverging semiangles. Bartz,[2] for example, conducted his experiments with a nozzle which had semiangles 30° and 15°, respectively. The results are valid only qualitatively at larger semiangles. The method of optimization follows the classical method of Euler using a Lagrange undetermined multiplier. The resulting equations, which are complicated, have been solved numerically by assuming several convergent sections. The results show that a steep concave inlet is the best from the stand-point of heat transfer.

Analysis

The assumptions made herein are 1) the flow is "one-dimensional" and in steady state; 2) the nozzle is axisymmetric; 3) there is no axial heat conduction; 4) ideal gas with frozen composition; 5) Pr = 1; and 6) T_w = const.

The equation for change of enthalpy per unit mass along the nozzle is[3,4]

$$dq_m = c_p dT + VdV = c_n dT \tag{1}$$

where

$$c_n = c_p(n - \gamma)/[\gamma(n - 1)] \tag{2}$$

By introducing a definition of a local total temperature

$$T_0 = T + V^2/(2c_p) \tag{3}$$

one gets from Eq. (1)

$$dq_m = c_p dT_0 = c_n dT = c_p dT + VdV \tag{4}$$

which follows $dp_0 = 0$.